Microstructure of as-polymerized thermoplastic polyurethane elastomers

Michael A. Vallance*, Janis L. Castles and Stuart L. Cooper†
Department of Chemical Engineering, University of Wisconsin, Madison, Wisconsin 53706, USA
(Received 3 October 1983)

Ten segmented polyether–urethane thermoplastics were studied in the as-polymerized state. Polyether-segment, number-average molecular weight and molecular weight distribution were varied among the set of polymers, as were the molar ratios of diisocyanate to diol chain extender to polyether glycol. Experimental techniques included differential scanning calorimetry, dynamic mechanical analysis, volume-temperature measurements, X-ray diffraction and hot-stage, polarized-light microscopy. At room temperature the materials possessed non-impinging spherulites, about 10 μm in diameter, in a non-birefringent matrix. X-ray diffraction from these same films showed no crystallinity, except in two cases. The spherulites irreversibly disappeared in the temperature range 350–400 K, accompanied by sharp decreases in dynamic modulus and a small thermal transition. Thermal disruption of urethane-dominated domains was observed at considerably higher temperatures, from 400–520 K, depending on molecular structure. Polyether crystallite melting was seen only below 305 K. These observations can be explained by a polymerization-solidification scenario which assumes: (1) de-mixing of isocyanate-capped prepolymers to form spatial gradients based on the urethane weight fraction of the prepolymer chains, and (2) decomposition of the polymerizing melt by nucleation and growth on a molecular scale to form polyurethane-rich spherulites during the reaction.

(Keywords: thermoplastic elastomer; spherulite; reaction moulding; segmented polyether–urethane)

INTRODUCTION

Segmented polyurethane thermoplastics, filled and unfilled, serve well as elastomers in applications where strains are moderate and strain rates are low. Structurally, these polymers consist of polyurethane sequences, usually aromatic, interspersed with polyether or polyester sequences, usually aliphatic. Although light crosslinking is employed in many commercial applications, the elastomeric properties are due primarily to domain formation in the solid state. A rigid, cohesive, polyurethane-rich dispersoid in the viscoelastic medium provides increased modulus and elastic recoil by serving both as filler and labile network points. By controlling the distributions of polyurethane and polyether or polyester sequence lengths, the extents of chemical segregation and the nature of microstructure can be modified, leading to changes in mechanical properties.

Although injection moulding of such polymer systems is often employed, excessive melt viscoelasticity and thermo-chemical degradation of the polymer are problems that limit the effectiveness of the technique. For bulk shapes, reaction injection moulding (RIM) has been realized as an alternative. The low-molecular-weight, low-viscosity reactants are injected into the mould at temperatures considerably lower than the melting point of the polymer. The reaction and solidification processes proceed simultaneously, initiated during the impingement mixing of the reactants.

RIM components can develop unique microstructures. Thermal gradients during the exothermic reaction–solidification process can result from heat-transfer limitations, and partial de-mixing of thermodynamically incompatible reactants is possible. Due to low viscosity early in the reaction, higher levels of phase separation are achievable than in microstructures formed by quenching the polyurethane melt. These microstructures, to a large extent, are duplicated in segmented polyurethane films polymerized in the mould in the absence of solvents, if stirring is limited to the initial times. Such 'as-reacted' or 'reaction-moulded' films, if reacted in very shallow moulds, do not develop significant temperature gradients during polymerization. The resultant films exhibit homogeneous microstructures more suitable for morphological examination, as compared to RIM bar specimens.

Reaction-moulded polyurethane elastomers develop unique microstructures, and these have been studied by a number of investigators. Schneider *et al.*[1] studied segmented polyether-urethanes synthesized from methylenebis(4-phenylisocyanate) (MDI), 1,4-butanediol (BD) and a hydroxy-terminated 2000 molecular weight ABA block polyether, where A represents poly(ethylene oxide) and B represents poly(propylene oxide). The chain extender BD was added in a second step, and the polymers were cured at 373 K. Sample compositions varied from MDI:BD:polyether glycol ratios of 2.1:1:1 to 6.3:5:1. Transmission electron microscopy (TEM) and polarized-light microscopy revealed the presence of spherulites for all compositions; their volume fraction increased with increasing polyurethane weight fraction. Crystalline diffraction was absent in the compositions lowest in polyurethane fraction, but could be seen in compositions

* Present address: General Electric Co., Research and Development Center, Schenectadt, New York, USA.
† Author to whom correspondence should be directed.

0032-3861/84/121734-13$03.00

with higher polyurethane contents. The authors concluded that the microstructures consisted of stacked polyurethane crystalline lamellae interspersed with layers of amorphous polymer within the fibrils of the spherulites, and dispersed polyurethane domains in a polyether matrix elsewhere.

Chang and Thomas[2] reported on an investigation of as-reacted segmented polyester–urethanes made in a one-step batch reaction from MDI, BD and a polydisperse, 2000 molecular weight, hydroxy-terminated polycaprolactone (PCL). The curing temperature was 418 K. The compositions varied in their MDI:BD:PCL ratios from 1:0:1 to 6:5:1. For as-reacted compositions from 2:1:1 to 6:5:1, evidence for polyurethane crystallinity was seen with differential scanning calorimetry (d.s.c.) in the form of melting endotherms during heating with maxima from 479–494 K. Diffraction lines due to polyurethane crystallinity were observed for compositions of higher polyurethane fraction, starting with 3:2:1. These lines were absent when the same polymers were dissolved in dimethyl formamide and cast at 325 K, which is above the polyester melting point, approximately 313 K for these copolymers. Trends in diffraction-line width and melting-point depression for the as-polymerized samples suggested that polyurethane crystallite size increased with increasing polyurethane fraction and, from heat of fusion measurements, so did overall crystalline mass fraction.

A segmented polyester–urethane was reaction injection moulded from a 6:5:1 mixture of MDI, BD and 2000 number-average molecular weight PCL using dibutyltin dilaurate as the catalyst described by Fridman *et al.*[3]. Plaques were made in a 1.27 cm thick mould whose walls were held at 358 K in one case and 310 K in another. The exothermic reaction to form urethane linkages caused large temperature gradients to occur across the mould's thickness during the course of the reaction. These temperature gradients were responsible for the formation of distinctly different microstructures and molecular-weight distributions at the plaques' centrelines and surfaces, as discerned by d.s.c., X-ray diffraction, intrinsic viscosity measurements and gel permeation chromatography (g.p.c.). Hard segment crystallinity was evident by d.s.c. at both positions in both samples. Using TEM and polarized-light microscopy it was possible to identify spherulites and electron-dense globules, which were thought to be glassy polyurethane-rich regions.

As-reacted morphologies were investigated by Chang *et al.*[4] in a series of one-step, batch-reacted, segmented polyether–urethanes synthesized from MDI, BD and the 2000 molecular-weight, hydroxy-terminated ABA block polyether described earlier. MDI:BD:polyether glycol ratios were varied over the broad range 1.8:0.7:1 to 24.8:22.8:1, and dibutyltin dilaurate was added as a catalyst. Plaques, 0.32 cm thick, were cured at 373 K. All samples but that with the lowest polyurethane content displayed spherulites, while those with relatively high polyurethane content exhibited distinctive skin-core microstructures across the plaques' thicknesses, with a dearth of spherulites in the interior. D.s.c. heating traces exhibited polyurethane melting endotherms characteristic of crystalline and paracrystalline ordering, except in the systems relatively low in polyurethane fraction. Crystalline diffraction lines were observed to diminish in intensity and vanish with decreasing polyurethane fraction, in agreement with d.s.c. measurements. Substantiating their light-microscope observations, these investigators found distinct differences in d.s.c. traces from skin and core regions of the materials with high polyurethane fractions. TEM investigations revealed two types of hard-segment rich spherulites, differing in internal organization, as well as hard-segment rich globules reminiscent of those in a previously referenced study[3]. The skin-core microstructures in the polyurethane-rich samples were again related to temperature gradients early in the polymerization process. Higher temperature towards the middle of the mould increased the mobility of the growing chains and fostered better mixing. The lack of spherulites in the interior was ascribed to the lack of MDI-rich centres.

Carmargo and co-workers[5] studied RIM segmented polyether-urethanes from the same chemistries as those of refs. 1 and 4. Polyurethane fraction, mould temperature and catalyst concentration were varied between samples. Dynamic mechanical analysis (DMA) suggested better phase separation in the slower-reacting, uncatalysed reactions. This result was supported by X-ray diffraction measurements which showed strong polyurethane diffraction lines from uncatalysed samples and weak lines from catalysed samples. Polarized-light microscopy showed strong birefringence from uncatalysed samples and little birefringence from catalysed samples. Catalysed samples had higher molecular weights. The authors explained the microstructural differences between catalysed and uncatalysed polymers in terms of reaction temperatures away from the mould walls. High reaction rates in the catalysed reactions led to high reaction temperatures and lower viscosities, favouring homogeneous mixing of reactants, and less inhomogeneity in the resultant polymer solids.

The study of as-reacted microstructures in melt-polymerized segmented polyurethane elastomers is of interest for several reasons: (a) the microstructures resemble those found in commercial bulk shapes produced by RIM; (b) study of such microstructures can provide insights into the causative chain of events which occurred during the reaction-solidification process; and (c) the comparative study of these microstructures and those formed by melt and solution casting of comparable polymers affords us the opportunity to evaluate the role of processing in the determination of engineering properties.

The present study centres around the investigation of ten segmented polyether–urethane films in their as-reacted state. Whereas the previously referenced studies[1,2,4,5] were concerned with the effect of changing the polyurethane-sequence length distribution, this study focuses on the role of the polyether-sequence length distribution. The mechanical properties[6] and the dielectric properties[7] of these polymers have been reported on previously. In this study, d.s.c., DMA, hot-stage light microscopy, X-ray diffractometry, and dilatometry have been used to further understand the role of processing in forming thermoplastic elastomers.

EXPERIMENTAL

Synthesis

Poly(tetramethylene ether)glycol (PTMEG) was dried for 1 h at 358 K and 666 Pa (absolute). The calculated amount of MDI was then added to the PTMEG at 353 K under nitrogen with agitation. A slight endotherm subsided after 5 min. The reaction was then continued for 2 h

Table 1 Chemical parameters

Polymer Designation	Mole ratios MDI/BD/PTMEG	$\langle M \rangle_n$[a]	w_h[b]	$\langle M \rangle_\eta / \langle M \rangle_n$[c]
Q1	2.0/0.95/1	977	0.436	2.01
Q2	2.4/1.33/1	1785	0.326	1.52
Q3	2.4/1.33/1	1804	0.324	1.97
Q4	2.4/1.33/1	1850	0.318	2.75
Q5	2.5/1.425/1	2020	0.307	2.05
Q6	3.5/2.375/1	2020	0.383	2.05
Q7	2.9/1.805/1	2422	0.298	1.89
Q8	3.4/2.28/1	2915	0.292	2.35
Q9	5.8/4.56/1	5430	0.271	3.81
Q10[d]	3.6/2.47/1	2147	0.375	–
S1	2.0/1.0/1	1008	0.426	–

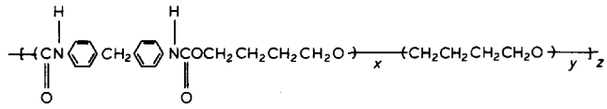

[a] $\langle M \rangle_n$ is the PTMEG number-average molecular weight
[b] w_h is the polyurethane weight fraction
[c] $\langle M \rangle \eta$ is a PTMEG viscosity-average molecular weight
[d] Ether segments are random copolymers of poly (tetramethylene oxide) and poly (ethylene oxide)

at 358 K under nitrogen with agitation. At the completion of this step the reaction mixture was degassed for 0.5 h at 666 Pa, still at 358 K, before adding the calculated amount of preheated BD (95% of the stoichiometric amount needed for complete reaction). The BD was injected by syringe. After stirring for 1 min the mixture clarified; stirring was continued for 1–3 min. The mixture was then poured into preheated moulds which were pressed at 383 K for about 17 h, then demoulded and stored at ambient temperature. Film thicknesses were typically 0.01 to 0.02 cm. No catalysts were used in either step. We are grateful to Dr E. Pechhold of E. I. du Pont de Nemours & Co., Inc., for supplying these materials to us.

Stoichiometries are listed in *Table 1* as are PTMEG number-average molecular weights $\langle M \rangle_n$ for the 10 samples. Note that sample Q10 differs in that the ether segments are random copolymers of poly(tetramethylene oxide) (PTMO) and poly(ethylene oxide). Also listed in *Table 1* are hard segment weight fractions w_h for the ten polymers. Polydispersity of the PTMEG's is measured by the ratio $\langle M \rangle_\eta / \langle M \rangle_n$ where $\langle M \rangle_n$ is the number-average molecular weight and $\langle M \rangle_\eta$ is a viscosity-average molecular weight:

$$\langle M \rangle_\eta = 3.39 \times 10^5 \eta^{0.493} \quad (1)$$

where η is the viscosity in N/cm^2/s of the 313 K melt. These ratios are also listed in *Table 1*. $\langle M \rangle_\eta / \langle M \rangle_n$ ratios of two typically correspond to $\langle M \rangle_w / \langle M \rangle_n$ ratios of 1.5, where $\langle M \rangle_w$ is the weight-average molecular weight[6].

For comparison, a single segmented polyether–urethane copolymer was synthesized via a two-step solution route. The MDI:BD:PTMEG ratios of 2:1:1 and the PTMEG number-average molecular weight of 1008 were chosen to be comparable to those of Q1. The solution-polymerized sample is designated S1. The solvent dimethylacetamide (DMAc) and the three reactants were degassed before use. After dissolving the MDI in DMAc (10% solution), the PTMEG was added at 303 K with constant stirring under nitrogen. Stannous octoate (M & T Chemicals) equivalent to 0.5% by weight of the combined MDI and PTMEG was added as a catalyst, the solution was brought to 333 K for 0.5 h, then returned to 303 K. The BD was diluted to 10% in DMAc, then slowly added to the reaction vessel while temperature was maintained near 303 K. When all BD was in solution, temperature was raised to 328 K for 0.5 h. After cooling, water was used to precipitate the polymer. Following decanting and drying, the polymer was dissolved in tetrahydrofuran (THF) (10% solution), and a film was formed by pouring the solution onto a clean mercury surface and slowly evaporating the THF at 297 K through a perforated aluminium seal.

Instrumentation

X-ray diffraction powder patterns were measured with a Picker 3668A symmetrical-reflection, scanning diffractometer with nickel-filtered radiation from a copper target in a sealed tube. The power section was operated at 35 kV and 0.015 A. Output from the photomultiplier tube was conditioned by a pulse-height discriminator and an amplifier with an effective 10 s time constant. The pulse-height discriminator was set to eliminate harmonics, electronic noise and escape peak phenomena from the output. The scan speed was set at 1.45×10^{-4} rad/s of scattering angle. The take-off angle was selected to produce line focus with an angular width of 1.7×10^{-3} rad at half intensity. Divergence and receiving slits were chosen to have 0.017 rad ranges, and the scattering slit width was 0.025 cm, wide enough to detect parafocused radiation from all depths of the polymer films over the angular range of interest, where the film thicknesses were typically 0.01–0.02 cm. Transverse divergence of the beam was minimized by stacks of Soller slits before and after the sample. The use of thin-film samples guaranteed that the scattering patterns were characteristic both of surface and interior microstructures, and reduced optical-broadening by maintaining a nearly parafocusing geometry. To quantify broadening artifacts, large grain powders of silicon and caesium chloride were adhered to glass forming layers with thicknesses in the same range as those of the polymer films. The crystalline reflections in the angular

range of interest, 0.1–0.6 rad, had typical half-intensity breadths of 3.5×10^{-3} rad. Digital records were corrected for dark current, main bean intensity, parasitic air scattering, linear-absorption coefficient and thickness[8].

DMA measurements were made with a Toyo Rheovibron DDV-IIC viscoelastometer which has been automated for stand-alone operation. The automation strategy differs somewhat from that of the IMASS Autovibron[9]. The automated DMA is designed to measure the complex tensile modulus E^* at discrete times during a constant-rate heating program (typically 2 K min^{-1}) at 11, 35 or 110 Hz. All control and monitoring is via an LSI 11/3 microcomputer. Operator communication is via CRT terminal; data and software are kept on flexible, magnetic discs. Temperature ramp control is enabled (heating only) on the range 100 to 600 K via pre-cooling with liquid nitrogen and two 50 Ω heating coils which are switched in and out by TTL-activated, solid-state relays. The decision algorithm is a derivative-control routine which accepts input from the computer's real-time clock and a digital thermometer with 1 K resolution. Data transfer to and from the thermometer is via TTL, parallel lines and conversion of BCD data is done with software. Because the force and displacement transducers of the DDV-IIC share certain signal conditioning electronics, it was decided to measure the two harmonic wave forms in time series. Automatic switching is enabled by mechanical relays and TTL-activated reed relays which act in cascade. Similar circuitry controls the test frequency function. The amplitude and phase (relative to a constant reference) of the two transducer signals are measured with a PAR 129A vector voltmeter whose two-channel output is converted and stored via 12-bit, A/D converters. These data are used to calculate E^*. Slight pretensioning of the sample, which is a thin film, is accomplished with a D.C. stepping motor which responds through its controller electronics to pulse input. Each step corresponds to a 5×10^{-4} cm change in specimen length (guage length is typically 3 cm). Pretensioning is done in closed-loop control where the force-transducer output is the monitored function. Timing functions such as pulse shaping and programmed delays rely on a 1 MHz programmable timer. Data are displayed on the CRT in real time and stored on disc. The data file is subsequently re-entered and plotted with a digital pen plotter. Owing to elimination of systematic errors in resolving phase shift, the accuracy in measuring the phase shift δ is ± 0.001 rad at 110 Hz, the test frequency used here. A continuous nitrogen purge originating from a heat exchanger was used to aid in temperature control and to reduce icing, H_2O absorption and oxidation. Long slender guage sections were used; sample stiffness was always below 100 N cm^{-1}. Load-frame compliance was measured by testing metal foils of known modulus, and data were subsequently corrected for this series compliance.

Pretensioning of the sample under computer control used a strategy which always maintained guage length just long enough to prevent buckling during the 'compressive' half of the strain-controlled dynamic cycle. Since the dynamic displacement amplitude used was 7×10^{-4} cm and the pretensioning resolution is 5×10^{-4} cm, where typical guage lengths are 2–4 cm, the instantaneous guage length data can be used as a measure of linear thermal expansivity $\partial L/\partial T$. Data are exhibited as $l(T)/l_0$, where l is the instantaneous guage length and l_0 is the guage length at 273 K.

Two polarized-light microscopes were used. Room-temperature micrographs were obtained using an Ernst Leitz Wetzlar system. 750X micrographs were recorded on ASA 400 Kodak Tri-X pan film using a Canon AT-1 35 mm camera. Films, 0.001–0.002 cm thick, were viewed normal to their surfaces. Hot-stage microscopy was done with a Unitron Series N binocular scope, a Unitron electric-resistance-heater hot stage, and a long-working-distance 20× objective. The water-cooled hot stage was continuously purged with nitrogen and a Fluke 2160A digital thermometer was used with a type T thermocouple in contact with the sample. The heating rate was manually controlled to approximately 2 K min^{-1}.

D.s.c. heating traces were recorded with a Perkin–Elmer DSC-2C differential scanning calorimeter interfaced with a Model 3600 Data Station using TADS software. Samples, 20–30 mg in mass, were contained in aluminium pans; an empty pan was used as the reference. Mercury and indium melting were used for temperature calibration and indium's heat of fusion was used for power calibration. The cell block was continuously purged with helium, the glovebox with desiccated air. Data were base line corrected. Initial data, recorded at 2.5 K min^{-1}, displayed unsatisfactorily low signal-to-noise ratios; all data shown were recorded at 20 K min^{-1}.

To ascertain that Q1 were indeed thermoplastics, 5% solutions were prepared at 298 K with THF and more polar *N,N*-dimethylformamide (DMF), and at 368 K with DMF. All ten polymers were seen to swell in DMF at 298 K after 24 h, but non formed clear solutions. The polymers did not dissolve in THF. At 368 K, all polymer dissolved in DMF forming clear solutions which remained after cooling to ambient temperature.

RESULTS AND ANALYSIS

Differential scanning calorimetry

D.s.c. traces, measured while heating from 130 K at 20 K min^{-1}, are shown in *Figure 1* for polymer Q1

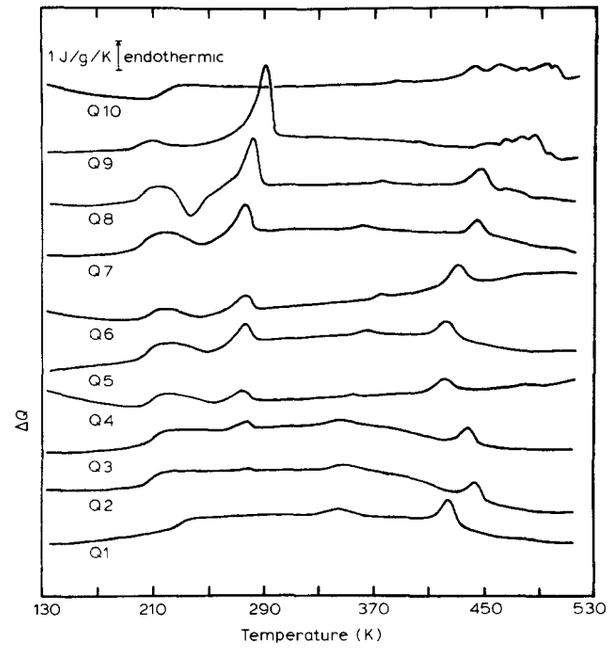

Figure 1 20 K min^{-1} d.s.c. heating traces for Q1 to Q10. Traces are shifted vertically for clarity

Table 2 Polyether sequence melting data

Sample	$\langle y+1 \rangle$[a]	T_g[b] (K)	T_e[c] (K)	Q_e[d] (J g^{-1})	T_a[e] (K)
Q1	10.6	229	–	0	236
Q2	19.6	212	291.5	1	214
Q3	19.8	206	288.3	2	210
Q4	20.3	202	293.3	7	211
Q5	22.2	202	293.7	15	210
Q6	22.2	198	293.9	15	210
Q7	26.7	197	296.3	26	202
Q8	32.2	195	297.9	33	203
Q9	60.1	189	304.9	64	206
Q10	–	213	–	0	223

[a] $\langle y+1 \rangle$ is the number-average degree of polymerization of the polyether sequences (see *Table 1*)
[b] T_g is an approximation of the glass transition temperature, taken as the inflection point of the base line shift
[c] T_e is a lower bound approximation of the equilibrium polyether melting point, measured as the upper point of tangency between the melting endotherm and the base line on 20 K min^{-1} heating traces
[d] Q_e is the area inside of the polyether melting endotherm normalized by the polyether segment mass
[e] T_a is the fictive glass transition temperature measured from the second E'' maximum in the dynamic mechanical data

through Q10. Events corresponding to the T_g in the polyether-dominated domains, exothermic polyether crystallization and endothermic polyether melting are seen at temperatures between 200 K and 310 K. The polyether crystallites formed during the heating program immediately following the thermal glass transition; the polymers had been quenched from 300 K to 130 K at 320 K min^{-1}. An exception is Q9; the majority of Q9's polyether crystallinity was present in the 300 K as-cast microstructure (see the X-ray scattering results). These data are summarized in *Table 2*. Q1, which was polymerized with very short polyether sequences, and Q10, which has noncrystallizable polyether sequences, do not show evidence of polyether crystallinity. Decreases in the number-average polyether degree of polymerization $\langle y+1 \rangle$ correlate with increases in the glass transition temperature and decreases in the polyether melting point T_e and the sensible heat of melting Q_e. This dependence of Q_e on $\langle y+1 \rangle$ may indicate that only the longer polyether sequences participate in crystallization, or it may be a measure of the polyurethane-segment concentration in the polyether-dominated regions[7,10].

Polyether melting-point depression with decreasing $\langle y+1 \rangle$ is expected, due to the necessary exclusion of polyurethane sequences from the polyether crystallites. Flory's melting point depression theory[11] is not strictly applicable here, because: the sequence length distribution is not known; and hindrance to polyether crystallite formation and re-organization during melting, due to the presence of polyurethane domains, is not embodied in the theoretical context. If it is assumed that the melting point is not particularly sensitive to the shape of the sequence length distribution, and that polyether crystallites form primarily in regions with few polyurethane domains; then Flory's model should apply. The case for equilibrium melting of one segment in a segmented copolymer has been given as[12]:

$$1/T_m - 1/T_m^\circ = -(R/h_u)[\chi(1-v_a)^2 + \ln p] \qquad (2)$$

where T_m = the equilibrium melting point
T_m° = the equilibrium melting point of the homopolymer
R = the gas constant
h_u = the heat of fusion per mole of structural units
χ = the liquid lattice heat of mixing parameter

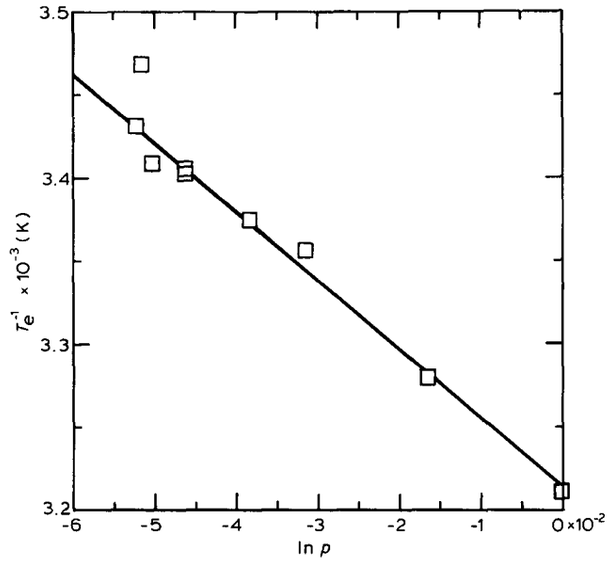

Figure 2 Polyether melting point as a function of polyether-segment degree of polymerization (see equation 3)

and v_a = the volume fraction of the liquid lattice occupied by the crystallizable component at $T = T_m$ for the case of vanishing crystallizable component

In calculating v_a, the polyurethane domains are neglected since they offer little surface area for interaction. Only the polyurethane segments which mix homogeneously on the liquid lattice are counted. The entropic term, written in terms of p, is based on an assumed geometrical distribution of lengths among the crystallizable component's sequences. In this case p is approximated by:

$$p \approx \langle y \rangle / \langle y+1 \rangle \qquad (3)$$

If the enthalpic term in equation (2) is very small relative to the entropic term ($\chi \to 0$ or $v_a \to 1$), then a linear relation between $1/T_m$ and $\ln p$ is predicted. *Figure 2* plots these two quantities, and a linear relation is in fact seen. Extrapolation to $p = 1$ yields $T_m^\circ = 311.2$ K which agrees with at least one literature value[13], 311.4 K. The slope has been used to evaluate the heat of fusion h_u as 28.2 J g^{-1}

Table 3 Superstructure transition

Sample	T_c[a] (K)	T_v[b] (K)	r[c] (%)	T_s[d] (K)
Q1	345	347	50	378
Q2	352	350	22	373
Q3	348	349	22	378
Q4	350	250	18	380
Q5	361	360	20	391
Q6	375	372	18	393
Q7	362	362	17	384
Q8	374	376	15	408
Q9	397	398	7	418
Q10	392	388	7	396

[a] T_c is the temperature marking the apex of the superstructure transition, as measured during 20 K min^{-1} heating programs
[b] T_v is the temperature at the onset of the E' transition in the rubbery plateau
[c] r is the percentage of stiffness lost through the rubbery plateau E' transition
[d] T_s (± 5 K) is the temperature at which the spherulitic structures vanish while heating at 2 K min^{-1}

which compares poorly with a literature value of 120.5 J g^{-1}.[14] Similar tendencies have been observed at this laboratory when applying the model to polycarbonate melting in segmented BPA polycarbonate-poly(ethylene oxide) copolymers and to poly(tetramethylene terephthalate) (PTMT) melting in segmented PTMT-poly(tetramethylene isophthalate) copolymers. Good agreement between model and literature values was found for polyester melting in segmented PTMO–PTMT copolymers[12]. The discrepancies may be caused by an inability, in general, to detect the equilibrium melting points by d.s.c. For polydisperse segment lengths, as T approaches T_m from below the segments reorganize into wider lamellae which, due to limited availability of the longest crystallizable segments, results in a decreasing crystalline fraction. Thus as T approaches T_m the crystalline fraction should be vanishingly small, and its melting virtually impossible to detect. This experimental difficulty was noted by Flory[11].

In the temperature range between 345 K and 410 K, all ten as-polymerized polymers exhibited a thermal event which varied in nature from polymer to polymer. In some cases the transition appeared as a shallow endotherm, while in others the event is marked only by an abrupt change in base line slope. The temperatures marking the event's apex are listed in *Table 3* as T_c, where it is seen that there is a general trend toward higher temperature with increasing polyurethane segment length. A molecular interpretation of this transition is offered in the discussion section.

At temperatures between 410 K and 520 K, Q1 to Q10 all exhibited endotherms in their 20 K min^{-1} d.s.c. traces, signifying the disruption of ordered polyurethane domains. From Q2 to Q10 the temperature range of the endotherm is seen to drop to a minimum at Q4, then rise again with increasing segment lengths. No explanation has been found for the initial trend, although it is noted that the major architectural differences among Q2 through Q5 is in PTMEG polydispersity, which increases from Q2 to Q4, then decreases again in the case of Q5. Whereas Q1 through Q8 exhibit endotherms below 450 K with single maxima, Q9 and Q10 exhibit complex multi-peaked endotherms that extend almost to 420 K, the region in which the MDI/BD urethane homopolymer exhibits melting[15]. As verified by X-ray scattering measurements, only these two polymers exhibit room-temperature crystallinity in the as-polymerized microstructures. Several authors have stated that the low

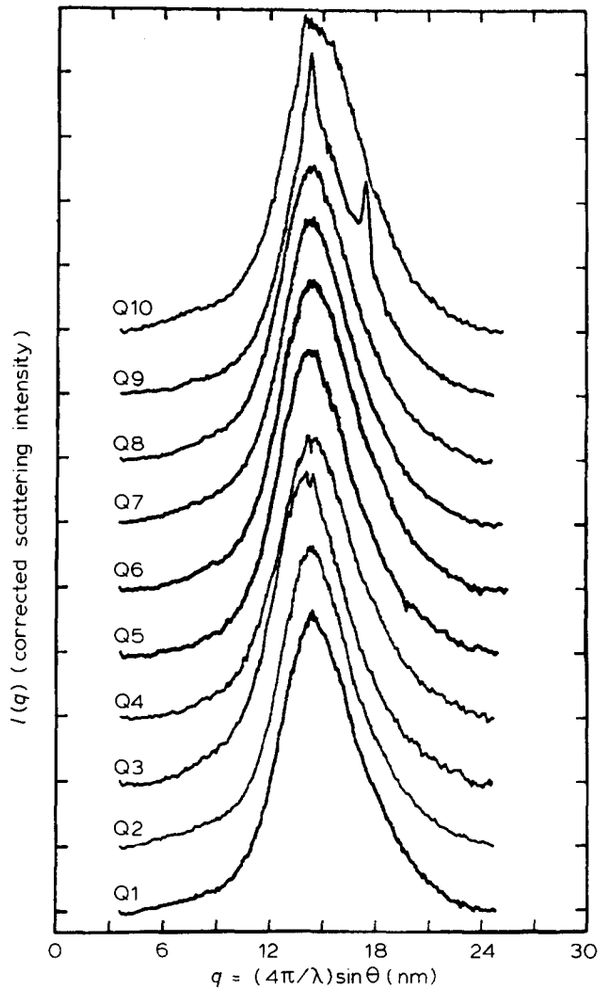

Figure 3 X-ray diffractometer powder patterns for Q1 to Q10. Patterns are shifted vertically for clarity

temperature of the melting endotherms typified by the Q1 to Q8 traces are evidence of inferior organization (paracrystalline ordering) in the polyurethane domains[1,16].

X-ray diffractometry

Corrected powder pattern scattering intensities are shown for all ten segmented polyether-urethane copolymers in *Figure 3*. The abscissa q is the magnitude of a

vector in reciprocal space:

$$q = (4\pi/\lambda)\sin\theta \quad (4)$$

where λ = the monochromatic excitation wavelength and 2θ = the scattering angle.

Only Q9 and Q10 exhibit evidence of crystalline diffraction. A PTMEG oligomer with number-average molecular weight 1000, was melted and re-solidified on a glass slide. The scattering pattern from this coating exhibited two strong diffraction maxima which corresponded in position (d-spacings of 0.441 and 0.363 nm) and relative intensity to the diffraction maxima apparent in the Q9 pattern. The diffraction lines in Q10, although not distinct are typical of polyurethane crystallinity in such polymers[3,16]. Three diffraction lines are apparent with d-spacings of 0.784, 0.456 and 0.379 nm. These same three lines are apparent in the Q9 pattern, although the two higher-angle lines appear as shoulders on the strong polyether lines.

Chang *et al.*[4] in their study of segmented polyether–urethanes found no X-ray diffraction evidence for polyurethane crystallinity in polymers with compositions 1.7:0.7:1 and 2.8:1.8:1 (MDI:BD:oligomeric polyether glycol). They did find such evidence in systems with longer polyurethane sequences, starting with composition 4.2:3.2:1, where the three polyurethane diffraction lines were seen. In the present study, these three lines are seen in Q9 (5.8:4.56:1) and Q10 (3.6:2.47:1), although they are very small relative to the amorphous background scattering. All polymers with shorter polyurethane sequences, starting with Q6 (3.5:2.38:1), exhibit no crystalline diffraction lines. There is concurrence between the scattering and d.s.c. measurements, with only Q9 and Q10 exhibiting melting endotherms between 500 and 520 K. Further, only Q9 exhibited polyether melting without first demonstrating a crystallization exotherm, suggesting that only Q9 possesses polyether crystallinity at 298 K prior to quenching.

Dynamic mechanical analysis

In-phase (E') and quadrature (E'') components of the complex tensile modulus are shown in *Figures 4–7* as a function of temperature during 2 K min^{-1} heating from 123 K.

Figure 4 shows E' data for Q2 through Q5; E'' data have been omitted for clarity. All four materials exhibit glass transitions ostensively in the ether-dominated domains which begin at 185 to 187 K. The glass-transition temperature of the polyether homopolymer has been reported as 185 K[14]. During heating through the glass-transition region, the polyether sequences gain mobility and crystallize, then subsequently melt with further heating. This results in a shoulder on the glass transition between 226 K and 295 K[17]. The size of the shoulder increases dramatically with the average degree of polymerization of the polyether sequences $\langle y+1 \rangle$, even though the variation in $\langle y+1 \rangle$ is small, from 19.6 in Q2 to 22.2 in Q5. Heat of melting measurements confirm a 15-fold increase in crystallinity between Q2 and Q5. The shoulders disappear at temperatures between 290 and 295 K, corresponding to the upper melting point (T_e) data in *Table 2*. The moduli in the rubbery plateau region from 295 to 395 K change relatively little. Close observation shows that three of the four polymers exhibit moduli that rise with increasing

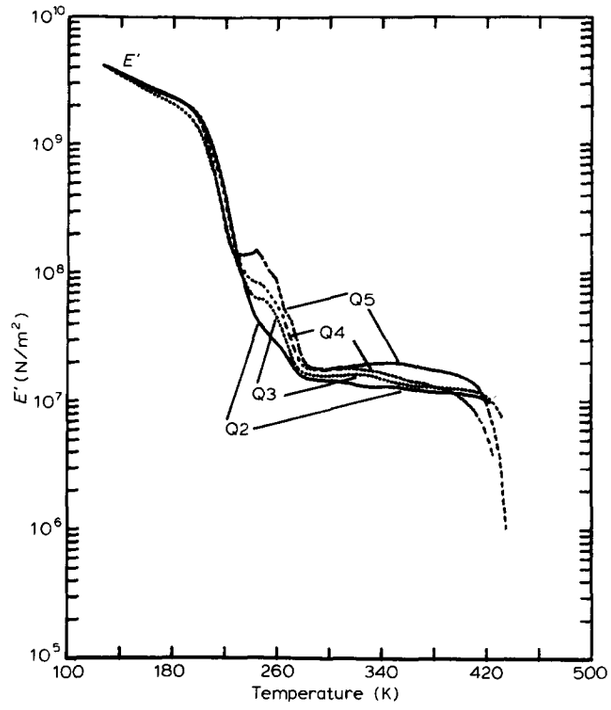

Figure 4 Dynamic tensile storage modulus data for Q2, Q3, Q4 and Q5 at 110 Hz and 2 K min^{-1}

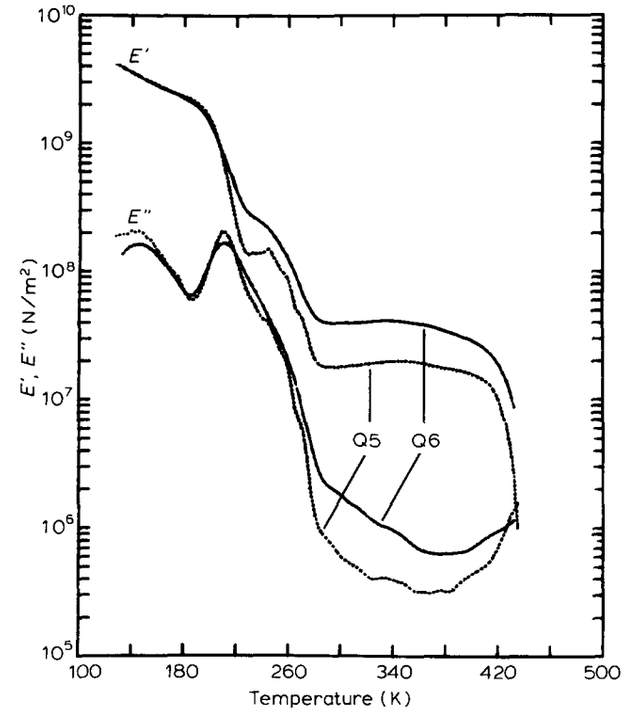

Figure 5 Dynamic tensile storage and loss moduli data for Q5 and Q6 at 110 Hz and 2 K min^{-1}

temperature in portions of this region, much as in covalently bonded, elastomeric networks[18]. The modulus values in the rubbery plateau region vary with average polyether-segment degree of polymerization; the highest modulus occurs in Q5, the system with the longest polyether segments, and so on. Interestingly, Q5 has the lowest polyurethane fraction of the four, 0.307 and Q2, with the lowest modulus, has the highest polyurethane fraction 0.326. At 350 K E' is 2.00×10^7 N/m^2 in the case

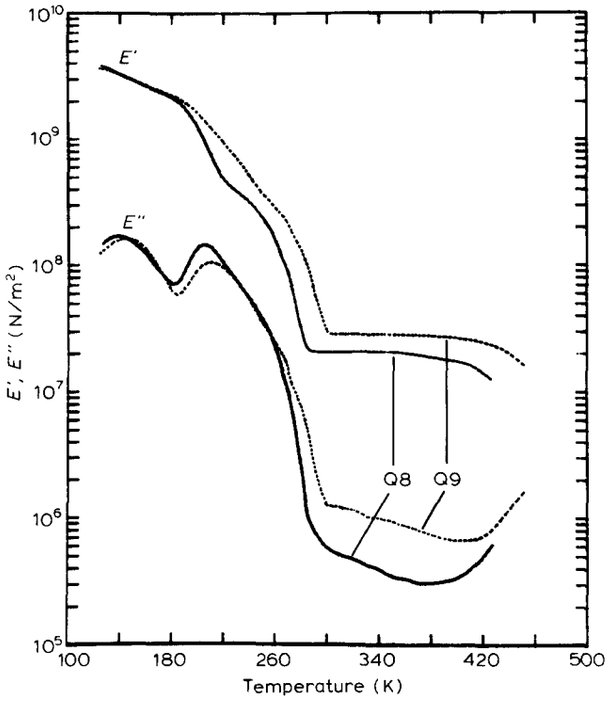

Figure 6 Dynamic tensile storage and loss moduli data for Q8 and Q9 at 110 Hz and 2 K min^{-1}

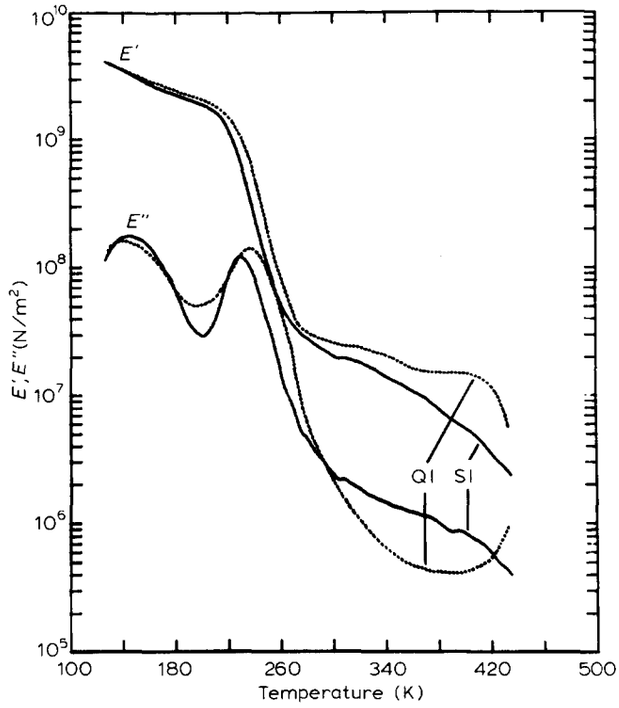

Figure 7 Dynamic tensile storage and loss moduli data for Q1 and S1 at 110 Hz and 2 K min^{-1}

of Q5, 1.31×10^7 N/m^2 for Q2, and intermediate to these values for Q3 and Q4. Above 395 K, polyurethane domains begin to disorder, resulting in softening; all four heating programs were terminated before 435 K. The onset of softening at 395 K, corresponds to the beginning of the polyurethane melting endotherms in *Figure 1*.

Figure 5 shows E' and E'' data for Q5 and Q6. The two data sets are similar except for the magnitudes of E' and E'' in the rubbery plateau region, both of which are higher in the case of Q6 due apparently to its higher polyurethane content: 0.383 for Q6 *versus* 0.307 for Q5. Both polymers are based on the same PTMEG batch. At 350 K the E' values are 2.00×10^7 N/m^2 for Q5 and 4.11×10^7 N/m^2 for Q6. The glass transition onset does not appear to differ much between the two samples. A broad E'' maximum in the glassy region is due to energy absorption by tetramethylene sequences in both polyether and polyurethane segments[19].

Q8 and Q9 data are displayed in *Figure 6*. As with Q2 through Q6, the onset of glass transition is apparent from these E' data at 185 K. Polyether melting persists to 304 K for Q9 and 294 K for Q8 in fair agreement with 20 K min^{-1} d.s.c. results. A striking feature in both cases is the abrupt transition between polyether melting and the rubbery plateau. The most apparent difference between Q8 and Q9 is in their E' and E'' rubbery plateau values. E' is 2.80×10^7 N/m^2 at 350 K for Q9 but only 2.07×10^7 N/m^2 for Q8. The polyurethane weight fractions for these two polymers are similar: 0.271 for Q9 and 0.292 for Q8. At 400 K Q8 begins to exhibit substantial softening, but Q9, which possesses appreciable polyurethane crystallinity did not begin to soften until 420 K.

It appears that at constant weight fractions of polyurethane and polyether increasing the average polyether and polyurethane-segment lengths serves to enhance the rubbery plateau modulus[20]. Similarly, given a constant distribution of polyether segment lengths, increasing average polyurethane segment length and polyurethane weight fraction tends to increase the rubbery plateau modulus.

In *Figure 7* dynamic mechanical data for Q1 and S1 are compared. Striking differences are noted between data for the melt-polymerized film and the solution-polymerized, solvent-cast film. Both films exhibit glass transition onsets at 208 K, a considerably higher temperature than for the other films in this study (Q10 excepted). The E' curve for Q1 exhibits only a trace of a shoulder between 250 and 272 K, related to polyether crystallinity; no polyether melting could be detected by d.s.c. in the cases of Q1 or S1. Throughout the rubbery plateau region Q1 consistently performs better than S1, exhibiting both higher storage modulus and lower quadrature component. At 350 K, E' is 1.24 N/m^2 for S1 relative to 1.85 N/m^2 for Q1. Furthermore, the curve shapes are distinctly different. S1 exhibits continuous softening throughout the rubbery plateau region; E' drops from 3.51×10^7 N/m^2 at 270 K to 0.54×10^7 N/m^2 at 400 K, an 85% decrease. In the same temperature range, Q1's E' remains relatively constant, first showing signs of softening above 410 K, near the temperature at which the polyurethane melting endotherm becomes apparent by d.s.c. At 295 K Q1 is a lively elastomer, whereas S1 is relatively compliant with highly damped recoil.

All E'' thermomechanical data exhibit two maxima, one in the glassy-response temperature range and one located near T_g on the temperature scale. This second maximum is often regarded as a fictive value for T_g. For comparison, it has been tabulated in *Table 2* as T_a. Although T_g and T_a in *Table 2* exhibit similar trends, T_a is always higher, by 2–17 K. It may be that the E'' shoulder due to polyether crystallization causes the apparent shift in T_a.

Although difficult to discern on the semi-logarithmic plots of *Figures 4–7*, all ten as-polymerized films went

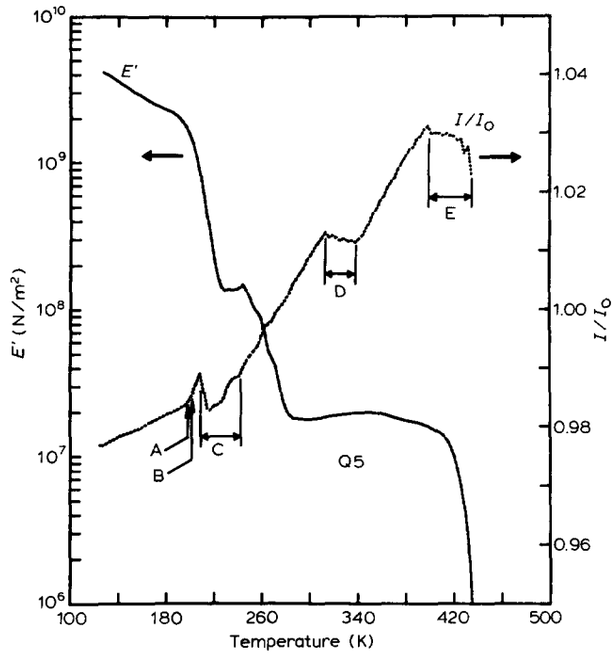

Figure 8 Dynamic tensile storage modulus and normalized gauge length for Q5 at 110 Hz and 2 K min^{-1}

through a distinct transition to lower E' in the temperature range 350–410 K. Generally, the onset temperature T_y is seen to move to lower temperature and the percentage decrease r in E' across the transition increases as the average polyurethane-segment length decreases. These trends are tabulated in *Table 3*. T_y is nearly identical with T_c in every case (where T_c was measured from d.s.c. traces). Further evidence for this transition was seen by microscopy. A possible mechanism for the phenomenon is proposed in the discussion section.

Volume–temperature analysis

E' and l/l_0 are plotted as a function of temperature for Q5 in *Figure 8*. The $l(T)$ data for the other nine polymers are similar to that for Q5. The point where the slope of $l(T)$ changes abruptly, labelled A, corresponds to the glass transition temperature of the polyether-rich phase. Point B is the T_g value estimated from the inflection point in the d.s.c. trace; agreement between the two is fair. In range C, the guage length decreased abruptly, then began to rise again, corresponding to the changes in volume accompanying polyether crystallization and subsequent melting. In range D, $l(T)$ exhibits a slightly negative slope while E' rises slightly with increasing temperature. In this temperature range, where no microstructural changes are occurring, the viscoelastic phase apparently follows classical rubber elasticity, which predicts positive $\partial E'/\partial T$ and negative $\partial l/\partial T$[18,21]. Range E again exhibits decreasing length with increasing temperature, most likely due to loss of dimensional stability at the onset of flow.

Optical microscopy

Figures 9–13 are polarized-light micrographs of Q2, Q3, Q6, Q7 and Q8. They are typical of all ten films, in that they exhibit non-impinging spherulites about 10 μm in diameter. No through-thickness microstructural variations were expected, since the films were only 10–20 μm thick and the uncatalysed reactions proceeded relatively

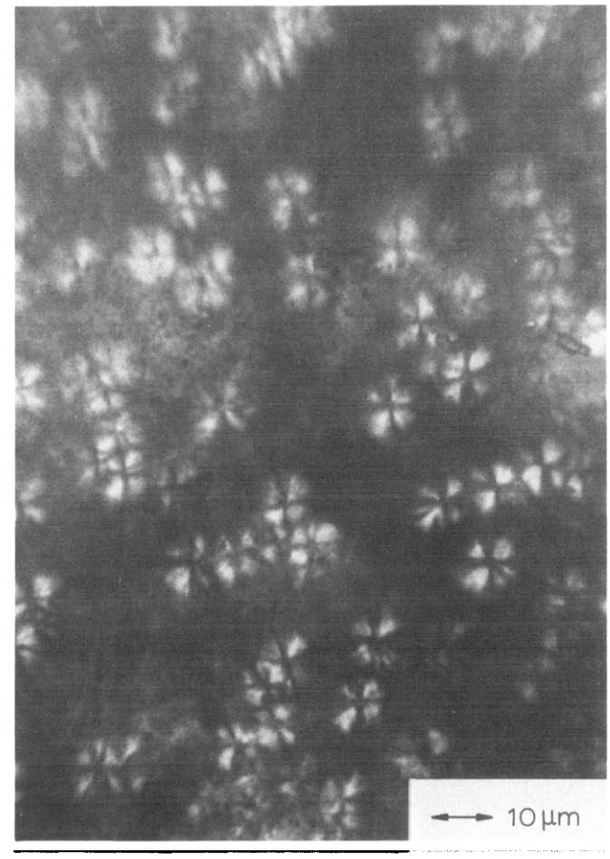

Figure 9 Optical micrograph of Q2 at 297 K as viewed between crossed polarizers

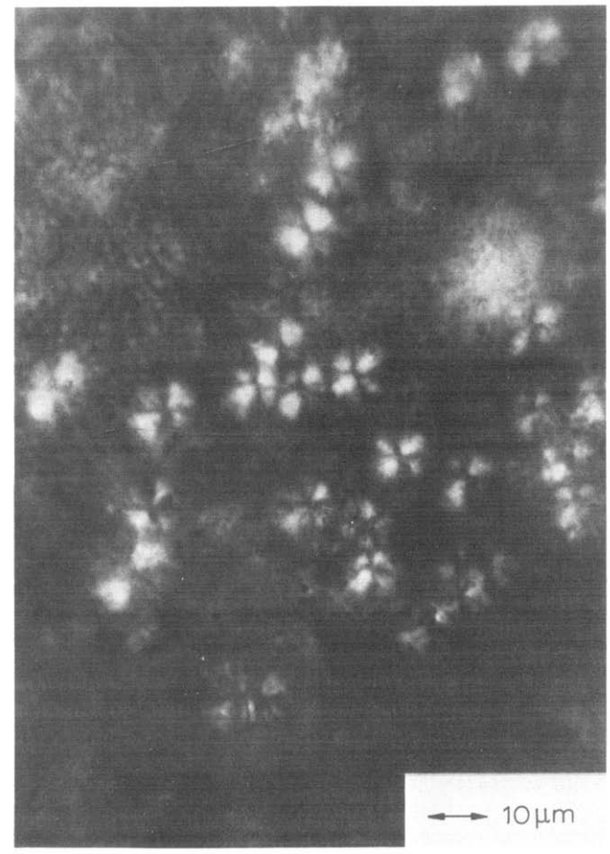

Figure 10 Optical micrograph of Q3 at 297 K as viewed between crossed polarizers

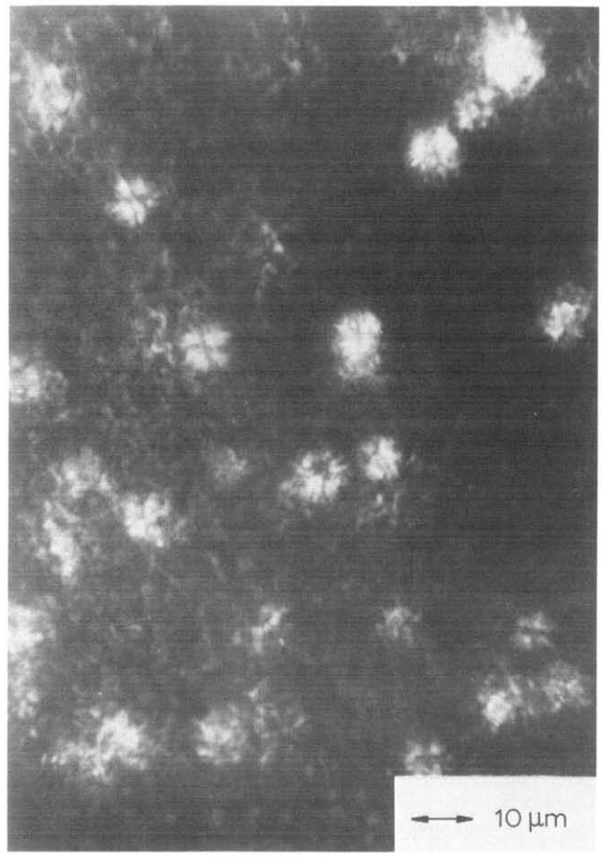

Figure 11 Optical micrograph of Q6 at 297 K as viewed between crossed polarizers

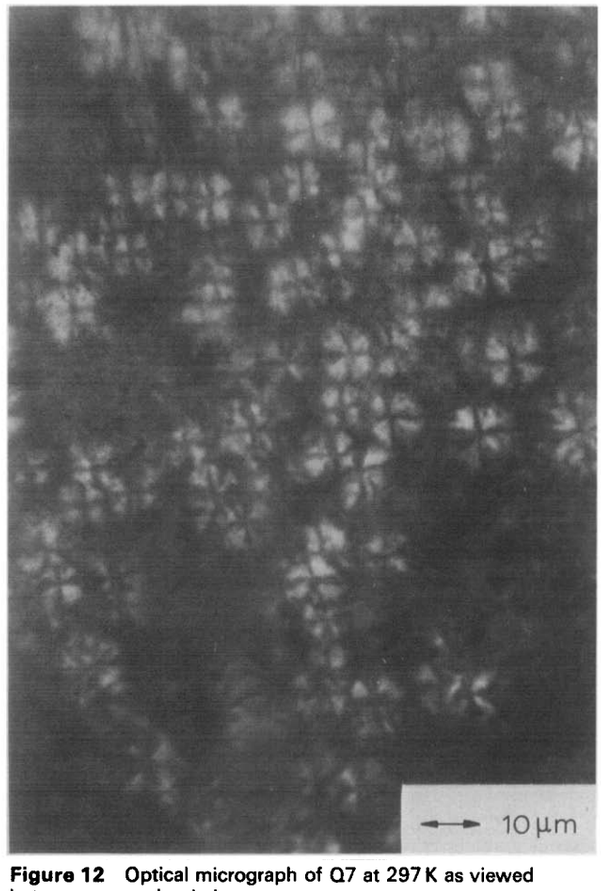

Figure 12 Optical micrograph of Q7 at 297 K as viewed between crossed polarizers

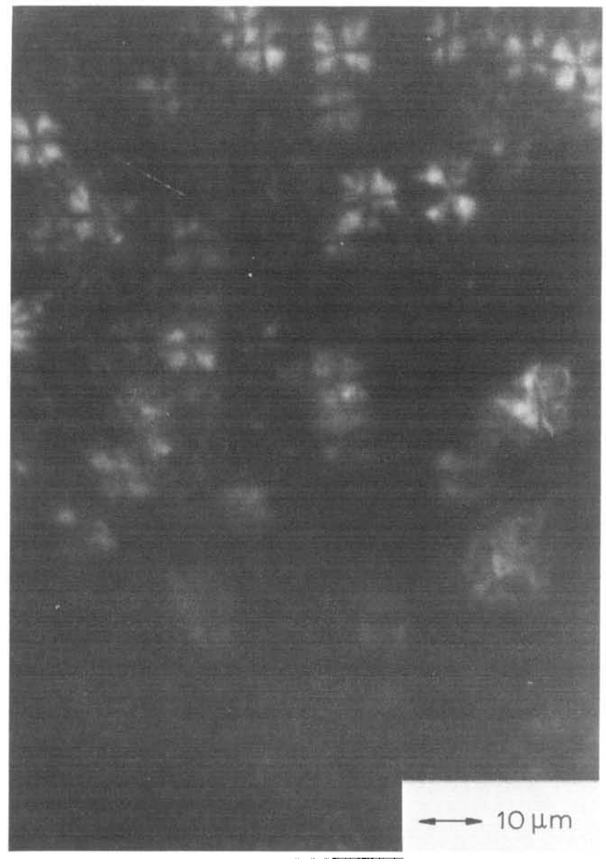

Figure 13 Optical micrograph of Q8 at 297 K as viewed between crossed polarizers

slowly[4,5]. S1 was optically clear and gave no evidence of spherulites between crossed polars.

The same polymer films were heated at 2 K min^{-1} from 300 K on the microscope stage. The following events were seen:

1. Between 300 and 350 K the existing spherulites became brighter in most cases.
2. Between 350 and 400 K, depending on the polymer, the spherulites began to lose intensity. They tended to all disappear within a few degrees of one another, leaving bright particles, about 1 μm in diameter, where their centres had been. The spherulites seemed to disperse starting from the outside.
3. Between 400 and 450 K, the films began to flow, as shown by rapid motion of the remaining bright particles.

The bright 1 μm particles may have been dust or other impurities. The temperatures T_s corresponding to the disappearance of all spherulites in the view field have been tabulated in *Table 3*, although the values are probably only reliable to ± 5 K. The values are similar to the temperatures at which the E' rubbery-plateau transitions end. The superstructure transformation described here was not reversible. Subsequent cooling, using a range of rates, from temperatures just above the transition, did not nucleate spherulitic growth.

The temperature range where the spherulites are seen to vanish, 350–400 K, is considerably higher than that for polyether melting which occurred below 305 K. There appears to be no correlation between the presence or absence of crystallinity, as measured by d.s.c. and X-ray diffraction, and the apearance of spherulites—all ten segmented polyether-urethanes in this study exhibit such

structure. Upon heating, the spherulitic textures do not vanish in the temperature range of polyurethane melting, but rather at somewhat lower temperatures. The disappearance of the spherulites is accompanied by a thermal transition and a distinct decrease in storage modulus. The temperature for this transition varies from polymer to polymer, showing a strong correlation with polyurethane-segment, number-average degree of polymerization $\langle x \rangle$. As $\langle x \rangle$ decreases, so too does the transition temperature, from 397 K for Q9 ($\langle x \rangle = 5.8$) to 345 K for Q1 ($\langle x \rangle = 2.0$). These temperatures would be reasonable values for the thermal glass transition temperature of a phase dominated by polyurethane sequences, but diluted with some polyether. The MDI/BD homopolymer glass transition temperature has been stated as 398 K[15].

DISCUSSION

In order to unify these observations, it is necessary to consider the sequence of events which occur during the polymerization–solidification process. In the first step excess MDI is reacted with PTMEG, so that after reaction the mixture consists primarily of MDI and diisocyanate oligomers of the form:

$$AB(CB)_mA,$$

where A is 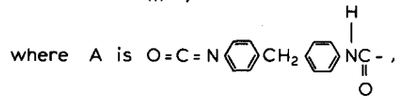 ,

B is 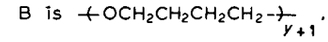 ,

and C is 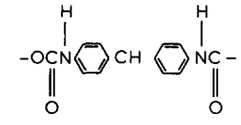 ,

where m can be 0. In the second step BD is added as the chain extender. Although stirring (or impingement mixing in the case of RIM) may result in an initial mixture which is nearly homogeneous at a molecular scale, at later times thermodynamic forces should act to form concentration gradients on some local scale. MDI and diisocyanate oligomers formed primarily from low-molecular-weight PTMEG will concentrate apart from oligomers formed primarily from high-molecular-weight PTMEG. Rigorous phase separation does not seem likely, in light of the continuous spectrum of compositions that would be present. The BD may or may not form preferential associations.

PTMEG-dominated regions would remain in a molten state throughout the reaction, since the reaction temperature 383 K is above the polyether homopolymer melting temperature 311 K, and the available polyurethane segments would be too short to form thermally stable domains. In the MDI-dominated regions, unreacted MDI could participate to form relatively long polyurethane sequences in the growing chains. As the concentration of 'high polymer' chains increased, it would become possible to nucleate a second phase in the MDI-rich regions.

The process is illustrated using the fictitious phase diagrams in *Figure 14*, where component 1 is a set of compositionally similar, MDI-dominated, oligomeric diisocyanates and component 2 is a set of compositionally similar, MDI-dominated, high polymers. Although present, the BD has not been specifically included. Since the

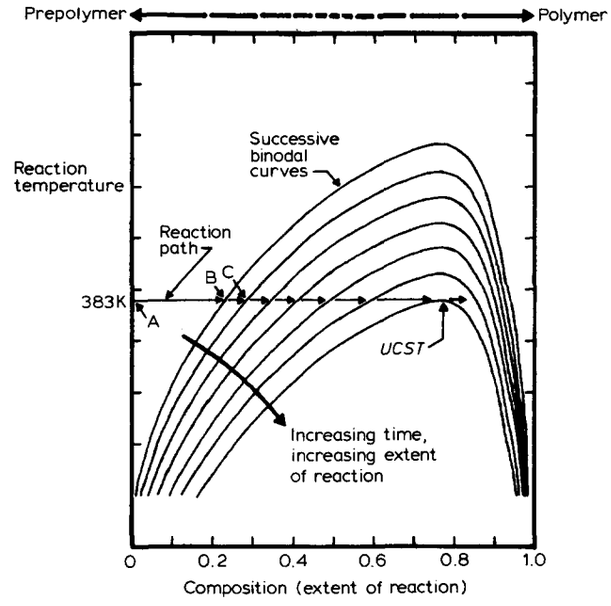

Figure 14 Representative phase diagrams at the melt-solid interface. Component 1 is the diisocyanate-capped oligomer. Component 2 is the segmented polyether–urethane copolymer. As polymerization proceeds and the spherulites grow, the binodal curve moves to successively lower positions. See text in the discussion section for a detailed description

distinction between growing oligomers and high polymers is not rigorous, the abscissa is better regarded as a measure of the extent of reaction than as a measure of the two fractions. The composition of both components 1 and 2, in terms of MDI and PTMEG is taken as that at the centre of the MDI-rich regions of the melt. The phase diagram has been drawn to exhibit upper-critical-solution-temperature (*UCST*) behaviour, since there is some evidence that elevated temperatures promote greater homogeneity[4,5]. *UCST* behaviour is typical of mixtures with positive heats of mixing.

Initially the mixture is at the reaction temperature and pure in component 1, the point labelled A in *Figure 14*. As the reaction proceeds, the composition moves towards the right. Eventually the composition path intersects the binodal curve at point B, and a high-polymer phase, relatively rich in MDI subsequently nucleates. The high polymer chains that phase separate form into solid domains with low chemical activity, so that the shape of the binodal curve is determined principally by the composition of the molten mixture at the solid–liquid interface. That composition becomes less and less concentrated in MDI as precipitation of the MDI-rich chains proceeds. The situation probably resembles that in *Figure 14*, where the binodal shifts to lower temperatures (e.g. from B to C) as the reaction proceeds. The molten mixture adjacent to the surface of the solid phase becomes increasingly concentrated in high polymer, while the high polymer being formed becomes increasingly dilute in MDI.

At some point the molten mixture would become upper critical, and thereafter the solidification process would halt. The reaction proceeds forward until the composition of the molten mixture is nearly pure in high polymer. Modest composition gradients would still exist in the molten state with polymers relatively rich in MDI near the solid–liquid interfaces and polyether-rich polymers

further away. Upon cooling it is unlikely that further separation on the molecular level would occur. By that time the composition (oligomer *versus* high polymer) of the molten phase will have moved far right of upper critical. Considerable cooling would be required before the composition–temperature curve would intersect the binodal, and then the polymer chains would be highly viscoelastic. Polyurethane sequences in the molten phase would be capable of microdomain formation on a nanometer scale, forming a labile network; and at lower temperatures polyether crystals could nucleate.

The solid domains, in the absence of shear, could be expected to grow in an isotropic fashion so that at any time the solid regions would be spherical in shape. For a polymeric molecule to condense from the molten mixture it would have to add onto the growing spherical region at the surface. The chain backbone could be expected, for the most part, to conform to and lie tangent to the existing surface, giving rise to spherulitic texture. This texture is not a consequence of crystallization, but rather is due to relatively amorphous isotropic phase growth. The poly urethane sequences of an adding chain will quite often find low energy, ordered or semi-ordered conformations involving other polyurethane sequences in the condensing chain or already on the surface. These ordered polyurethane domains would be surrounded by disordered, glassy regions containing both polyurethane and polyether sequences. The spherulites would be expected to exhibit radial compositon gradients, with MDI-rich chains near the centres.

Based on the model, it is expected that the spherulites should exhibit higher urethane content than the non-spherulitic regions and that the spherulites themselves should show gradients of composition, being richer in urethane linkages towards their centres. Electron microscopy studies[1,4] of electron density variation are in agreement with these predictions. If the spherulites are polyurethane-poor at their perimeters, then the perimeters would be less thermall stable. From hot-stage microscopy results, spherulites disorganize during heating through the polymerization–solidification temperature range, starting at the edge and moving inward.

The process whereby thermal disruption of spherulites occurs, is accompanied by a d.s.c. transition and a distinct dynamic mechanical transition at temperatures below the T_g temperature of the polyurethane homopolymer and below the temperatures where the ordered polyurethane domains are disrupted. A possible mechanism is the T_g of disordered polyether and polyurethane sequences within the spherulites. Besides affecting the thermo-mechanical transition, the intraspherulite, ordered polyurethane domains could then rotate and translate into lower-energy, non-spherulitic configurations, as observed. The temperatures where the thermal and mechanical transitions occurred were in good agreement for any one polymer. Across the ten polymers, this transition temperature tended to increase with increasing average polyurethane segment length. The incorporation of longer polyurethane segments tends to increase the polyurethane fraction in the spherulites, increasing the T_g temperature of the disordered fraction and the melting temperature of the ordered fraction.

The polyurethane-rich spherulites are expected to be resistant to solvent penetration, particularly for a non-polar solvent, at temperatures far below the T_g range of the disordered, intraspherulite material. The solubility studies support this prediction.

The importance of processing in the determination of useful engineering properties is graphically demonstrated by the comparison of dynamic mechanical properties between Q1 and S1, two polymers with nearly identical stoichiometries, but different synthesis and forming histories. The as-polymerized morphology of Q1 exhibits superior modulus and lower viscous dissipation over the entire useful temperature range, due in large part to its higher level of organization. The nature of the microstructure in polyurethanes melt-cast or solution-cast from non-polar solvents is in large part due to the high elasticity and viscosity present in the melt (or concentrated solution). These properties arise from the tendency of the polyurethane segments to be rodlike in their conformations[22], the effect of interchain hydrogen bonding, and possibly due to microphase separation in the molten state. These factors seem to prohibit long-range (μm) organization and decrease the overall degree of phase separation.

CONCLUSIONS

The role of processing parameters in determining chemical architecture, solid-state microstructure and engineering properties in segmented polyetherurethane copolymers is of singular importance. In particular, reactions in the mould, such as reaction injection moulding or melt polymerization, can lead to unique microstructures with desirable properties. This study has concluded, as have several in the past, that spherulite formation under such conditions is linked to spatial inhomogeneities in chain composition: polyurethane-rich chains are concentrated within the spherulitic regions.

The degree of ordering of which the polyether sequences are capable is found to increase dramatically with the average degree of polymerization of the sequences. This has been shown to relate to the requirement that polyurethane sequences be disallowed from participation in the polyether crystalline lattice. The breadth of the distribution of polyether sequences was not found to be strongly correlated with the measured properties. The ten as-polymerized segmented polyether–urethanes studied here exhibited excellent dynamic mechanical properties, with low dissipation factors and high, stable moduli in the rubbery-plateau temperature range. The value of the storage moduli tended to increase with increasing polyurethane fraction and with increasing average segment lengths, as might be expected.

The advantages of solvent-free, low-temperature, low-viscosity processing and superior mechanical properties due to high-level (10 μm) organization favour the use of segmented, polyurethane elastomers reacted in the mould for the manufacture of bulk elastomeric components.

ACKNOWLEDGEMENTS

The authors wish to thank Dr E. Pechhold of E. I. du Pont de Nemours & Co., Inc., for providing the polymer films of the Q series. We acknowledge the support of the Polymer Materials Program of the Division of Materials Research of the National Science Foundation through grant DMR 81-06888. Additionally one author (MAV) wishes to

thank the International Harvester Company and another author (JLC) thanks the National Science Foundation for providing graduate fellowships. Mr J. J. Hein provided us with the differential scanning calorimetry and Rheovibron measurements.

REFERENCES

1 Schneider, N. S., Desper, C. R., Illinger, J. L. and King, A. O. *J. Macromol. Sci.-Phys.* 1975, **B11**, 527
2 Chang, A. L. and Thomas, E. L. in 'Advances in Chemistry Series, No. 176, Multiphase Polymers', (Eds. S. L. Cooper and G. M. Estes), American Chemical Society, Washington, 1979
3 Fridman, I. D., Thomas, E. L., Lee, L. J. and Macosko, C. W. *Polymer* 1980, **21**, 393
4 Chang, A. L., Briber, R. M., Thomas, E. L., Zdrahala, R. J. and Critchfield, F. E. *Polymer* 1982, **23**, 1060
5 Camargo, R. E., Macosko, C. W., Tirrell, M. V. and Wellinghoff, S. T. *Polym. Eng. Sci.* 1982, **22**, 719
6 Pechhold, E. and Pruckmayr, G. *Rubber Chem. Technol.* 1980, **53**, 1032
7 Vallance, M. A., Yeung, A. S. and Cooper, S. L. *Colloid Polym. Sci.* 1983, **261**, 541
8 Alexander, L. E. in 'X-Ray Diffraction Methods in Polymer Science', Wiley, New York, 1969
9 Kenyon, A. S., Grote, W. A., Wallace, D. A. and Rayford, M. J. *ACS Polym. Prepr.* 1976, **17**, 7
10 Hu, C. B., Ward, Jr., R. S. and Schneider, N. S. *J. Appl. Polym. Sci.* 1982, **27**, 2167
11 Flory, P. J. *J. Chem. Phys.* 1949, **17**, 223
12 Vallance, M. A. and Cooper, S. L. submitted to *Macromolecules*
13 Wetton, R. E. and Allen, G. *Polymer* 1966, **7**, 331
14 Yoshida, S., Suga, H. and Seki, S. *Polym. J.* 1973, **5**, 25
15 MacKnight, W. J., Yang, M. and Kajiyama, T. *ACS Polym. Prepr.* 1968, **9**, 860
16 Bonart, R., Morbitzer, L. and Hentze, G. *J. Macromol. Sci.-Phys.* 1969, **B3**, 337
17 Lilaonitkul, A. and Cooper, S. L. in 'Advances in Urethane Science and Technology', Vol. 7, (Eds. K. C. Frisch and S. L. Reegen), Technomic, New York (1979)
18 Koshiba, M., Hwang, K. K. S., Foley, S. K., Yarusso, D. J. and Cooper, S. L. *J. Mater. Sci.* 1982, **17**, 1447
19 McCrum, N. G., Read, B. E. and Williams, G. in 'Anelastic and Dielectric Effects in Polymeric Solids', Wiley, London (1967)
20 Van Bogart, J. W. C., Gibson, P. E. and Cooper, S. L. *J. Polym. Sci. Polym. Phys. Edn.* 1983, **21**, 65
21 Flory, P. J. in 'Principles of Polymer Chemistry', Cornell University Press, Ithaca (1953)
22 Hwang, K. K. S., Wu, G., Lin, S. B. and Cooper, S. L., submitted to *Macromolecules*